RSCPublishing

COVER ARTICLE
Zhiguo Xia, Andries Meijerink *et al.*
Host composition dependent tunable multicolor emission in the single-phase
Ba$_2$(*Ln*$_{1-z}$Tb$_z$)(BO$_3$)$_2$Cl:Eu phosphors

PAPER

Host composition dependent tunable multicolor emission in the single-phase Ba$_2$(Ln_{1-z}Tb$_z$)(BO$_3$)$_2$Cl:Eu phosphors†

Zhiguo Xia,*[a] Jiaqing Zhuang,[a] Andries Meijerink*[b] and Xiping Jing[c]

A new strategy based on the host composition design has been adopted to obtain efficient color-tunable emission from Ba$_2$$Ln_{0.97-z}Tb_z$(BO$_3$)$_2$Cl:0.03Eu ($Ln$ = Y, Gd and Lu, z = 0–0.97) phosphors. This study reveals that the single-phase Ba$_2$$Ln_{1-z}Tb_z$(BO$_3$)$_2$Cl compounds can be applied to use allowed Eu^{2+} absorption transitions to sensitize Eu^{3+} emission via the energy transfer Eu^{2+} → (Tb^{3+})$_n$ → Eu^{3+}. The powder X-ray diffraction (XRD) and Rietveld refinement analysis shows single-phase Ba$_2$$Ln_{1-z}Tb_z$(BO$_3$)$_2$Cl. As-prepared Ba$_2$$Ln_{0.97-z}Tb_z$(BO$_3$)$_2$Cl:0.03Eu phosphors show intense green, yellow, orange and red emission under 377 nm near ultraviolet (n-UV) excitation due to a variation in the relative intensities of the Eu^{2+}, Tb^{3+} and Eu^{3+} emission depending on the Tb content (z) in the host composition, allowing color tuning. The variation in emission color is explained by energy transfer and has been investigated by photoluminescence and lifetime measurements and is further characterized by the Commission Internationale de l'éclairage (CIE) chromaticity indexes. The quantum efficiencies of the phosphors are high, up to 74%, and show good thermal stabilities up to 150 °C. This investigation demonstrates the possibility to sensitize Eu^{3+} line emission by Eu^{2+} via energy migration over Tb^{3+} resulting in efficient color tunable phosphors which are promising for use in solid-state white light-emitting diodes (w-LEDs).

1. Introduction

Solid state lighting (SSL) technology concentrating on white-light-emitting diodes (w-LEDs) is an important strategy for energy saving by replacing the conventional incandescent and fluorescent lamps.[1] The most promising approach to realize color stable w-LEDs is the combination of one or more phosphor materials with blue or near ultraviolet (n-UV) LEDs, known as phosphor-converted (pc) w-LEDs. Accordingly, much attention has been paid to finding new phosphors to improve the performance of w-LEDs.[2] Rare-earth ions are the most frequently used activators (luminescent ions) for phosphors due to the high efficiency and abundance of emission colors based on 4f → 4f or 5d → 4f transitions.[3] As a typical activator based on 5d → 4f emission, Eu^{2+} doped phosphors have been widely investigated because they usually have a strong broad

excitation band in the n-UV region (350–420 nm), and an intense emission which can vary from the UV region to the red region, depending on the host material.[4] The present generation of w-LEDs combines blue and yellow emission giving cold white light. There is a need for efficient red phosphors that can be excited in the n-UV or blue spectral region to realize efficient warm w-LEDs. A promising class of materials is based on emission of Eu^{2+} in (oxo)nitridosilicates, such as M$_2$Si$_5$N$_8$ and MSi$_2$O$_2$N$_2$ (M = Ca, Sr, Ba).[5] However, there are two drawbacks: the harsh synthesis conditions restrict synthesis to expensive industrial batch production and the red emission band is broad and extends beyond 630 nm where the eye sensitivity drops, reducing the lumen/W efficiency.[5] The holy grail in LED phosphor research is to find a narrow band emitter in the red spectral region, preferably around 610 nm. As is well-known in the lighting community, Eu^{3+} can produce efficient red emission around 610 nm due to the ^{5}D$_0$ → ^{7}F$_2$ transition and this has been applied for decades in commercial red phosphors like Y$_2$O$_3$:Eu^{3+} and Y$_2$O$_2$S:Eu^{3+}. It is of great interest to develop Eu^{3+} doped phosphors for LED applications, but the weak absorption of Eu^{3+} in the blue and n-UV region has limited use in practical LED systems.[6] Several approaches have been used to sensitize the Eu^{3+} emission, such as Mo^{6+}–O^{2-} or V^{5+}–O^{2-} charge transfer (CT) transitions in some Eu^{3+} doped molybdates or vanadates. This can be

[a]School of Materials Science and Technology, China University of Geosciences, Beijing 100083, P. R. China. E-mail: xiazg426@yahoo.com.cn
[b]Condensed Matter and Interfaces, Debye Institute for Nanomaterials Science, Utrecht University, Utrecht, The Netherlands. E-mail: A.Meijerink@uu.nl
[c]College of Chemistry and Molecular Engineering, Peking University, Beijing 100871, P. R. China
†Electronic supplementary information (ESI) available: Fig. S1–S5 will be available free of charge via the Internet. See DOI: 10.1039/c3dt32609h

effective for the enhancement of Eu^{3+} emission, but the luminescence efficiency for excitation in the n-UV region is low, especially at elevated temperatures.[7–8] Recently, Setlur proposed that $Ce^{3+} \rightarrow (Tb^{3+})_n \rightarrow Eu^{3+}$ energy transfer (ET) can give Eu^{3+} line emission after strong Ce^{3+} absorption in the n-UV and violet spectral regions making them potential candidates for n-UV and violet LEDs.[9] However, limitations related to the host lattice selection (*e.g.* Tb–Ce back transfer and quenching of the Eu^{3+} emission due to quenching *via* a metal-to-metal charge transfer (MMCT) state in Eu^{3+}–Ce^{3+} pairs) and a low thermal quenching temperature in the reported $Y_{0.493}Tb_{0.50}Ce_{0.002}Eu_{0.005}BO_3$ system restrict its further application.

An alternative approach is the use of Eu^{2+} as a sensitizer in europium doped materials containing Eu both in the 3+ and 2+ valence states. A great deal of work has been done on the partial reduction of Eu^{3+} and stabilization of both Eu^{3+} and Eu^{2+} in a single host lattice.[10,11] Therefore, in analogy to the $Ce^{3+} \rightarrow (Tb^{3+})_n \rightarrow Eu^{3+}$ system, $Eu^{2+} \rightarrow (Tb^{3+})_n \rightarrow Eu^{3+}$ ET is of great interest by the introduction of a mixed valence of Eu elements. Direct sensitization of Eu^{3+} luminescence by Eu^{2+} is inefficient due to the metal–metal charge transfer quenching.[12] In our previous work, we have developed a series of iso-structural $Ba_2Ln(BO_3)_2Cl$ (Ln = Y, Sm → Lu) compounds and Eu ions can be incorporated as Eu^{2+} on the Ba^{2+} sites and as Eu^{3+} on the Ln^{3+} sites for the $Ba_2Ln(BO_3)_2Cl$ (Ln = Y, Gd and Lu) system.[13,14] Red luminescence from Eu^{3+} with the aid of efficient ET of $Eu^{2+} \rightarrow (Tb^{3+})_n \rightarrow Eu^{3+}$ and Tb^{3+}–Eu^{3+} has been demonstrated in the $Ba_2Tb(BO_3)_2Cl$ compound.[14] Considering the versatile nature of the $Ba_2Ln(BO_3)_2Cl$ compounds, we propose a new strategy based on controlling the valence state of Eu and the energy transfer to Eu^{3+} by varying the Tb content in the host composition.[15] Accordingly, tunable multicolor emission from green to red, even full-color-emission in $Ba_2Ln_{0.97-z}Tb_z(BO_3)_2Cl$:0.03Eu ($Ln$ = Y, Gd and Lu, z = 0–0.97) phosphors can be realized upon n-UV excitation by using the allowed Eu^{2+} absorption transitions to sensitize Tb^{3+} and Eu^{3+} emission *via* ET of $Eu^{2+} \rightarrow (Tb^{3+})_n \rightarrow Eu^{3+}$. To the best of our knowledge, this investigation is a unique example of narrow-line emitting phosphors under broad-band n-UV or violet excitation allowing color tunability by controlled ET. The high quantum efficiency (QE) has also been investigated and values as high as 74% have been found making these phosphors promising candidates for use in w-LEDs.

2. Experimental section

2.1 Materials and synthesis

A series of iso-structural chloroborate compounds were prepared through solid state reactions, in which the formula of the Tb-free compounds is given as $Ba_{1.97}Ln(BO_3)_2Cl$:0.03Eu (Ln = Y, Gd, and Lu), and Tb-containing materials are designated as $Ba_2Ln_{0.97-z}Tb_z(BO_3)_2Cl$:0.03Eu ($Ln$ = Y, Gd, and Lu; z = 0.05, 0.10, 0.30, 0.40, 0.50, 0.60, 0.70, 0.90 and 0.97). The starting materials, $BaCO_3$ (99.95%), $BaCl_2·2H_2O$ (99.95%), H_3BO_3

(99.95%), were supplied by Sinopharm Chemical Reagent Co. Ltd, Shanghai, China, and rare earth oxides Y_2O_3, Gd_2O_3, Lu_2O_3, Eu_2O_3 and Tb_4O_7 with purity over 99.995% were supplied by China Minls (Beijing) Research Institute, Beijing, China. In a typical process, the starting materials were weighed in the proper stoichiometric amounts and 5% excess H_3BO_3 were added as flux. Then, they were thoroughly mixed in an agate mortar by grinding. After that, the mixture was fired in a crucible at 1000 °C in a reducing (N_2–H_2 = 95:5) atmosphere for 3 h. After cooling to room temperature, the final phosphors were obtained as microcrystalline powders.

2.2 Characterization

X-ray diffraction (XRD) patterns were measured on an X-ray powder diffractometer (XRD-6000, SHIMADZU, Japan), operating at 40 kV, 30 mA. The continuous scanning rate (2θ ranging from 10° to 70°) used for phase determination was 4° (2θ) min^{-1} and the step scanning rate (2θ ranging from 3° to 115°) used for Rietveld analysis was 8 s per step with a step size of 0.02°. The powder diffraction data were analyzed using a computer software General Structure Analysis System (GSAS) package.[16] The electron spin resonance (ESR, ER200-SRC-10/12) measurements at room temperature were carried out at X-band frequency to observe changes in the ratio of Eu^{2+}/Eu^{3+} ions. Diffuse reflection spectra on as-synthesized phosphors were measured on a UV-Vis-NIR spectrophotometer (SHIMADZU UV-3600) attached with an integrating sphere. $BaSO_4$ was used as a reference standard. The photoluminescence excitation (PLE) and photoluminescence (PL) spectra were recorded using a fluorescence spectrophotometer (F-4600, HITACHI, Japan) with a photomultiplier tube operating at 400 V and a 150 W Xe lamp was used as the excitation lamp. The temperature-dependence luminescence properties were measured on the same F-4600 spectrophotometer, which was combined with a self-made heating attachment and a computer-controlled electric furnace. Luminescence decay curves were obtained using a Lecroy Wave Runner 6100 digital oscilloscope (1 GHz) under excitation with a tunable laser (pulse width = 4 ns, gate = 50 ns, Continuum Sunlite OPO). The internal quantum efficiency was measured using the integrated sphere on the FLS920 fluorescence spectrophotometer (Edinburgh Instruments Ltd, UK), and a Xe900 lamp was used as an excitation source and white $BaSO_4$ powder as a reference to measure the absorption. The signals were detected by a Hamamatsu R928P photomultiplier tube.

3. Results and discussion

3.1 XRD refinement and phase structure

We have carefully synthesized $Ba_{1.97}Ln(BO_3)_2Cl$:0.03Eu and $Ba_2(Ln_{0.97-z}Tb_z)(BO_3)_2Cl$:0.03Eu ($Ln$ = Y, Gd, and Lu; z = 0.05–0.97). In our previous report, the successful isomorphic substitution for Ln^{3+} sites in the $Ba_2Ln(BO_3)_2Cl$ host by some trivalent rare earth ions, Y, Sm, Eu, Gd, Tb, Dy, Ho, Er, Tm, Yb, and Lu, was verified.[13] Fig. 1a gives the XRD patterns of
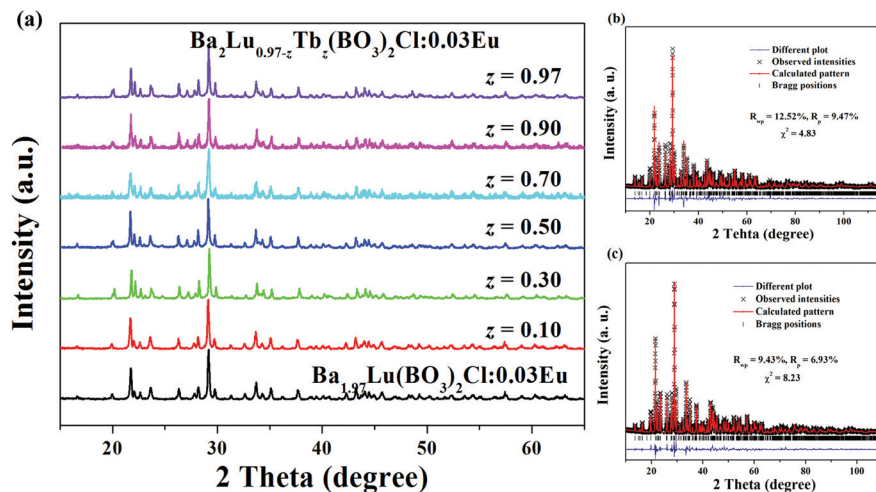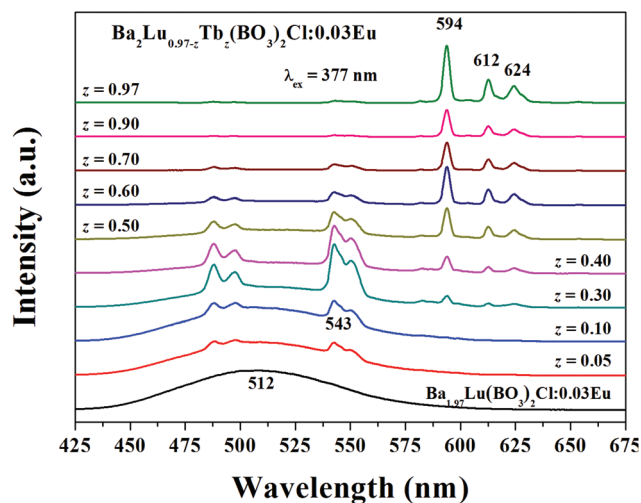
Fig. 1 (a) XRD patterns of $Ba_2Lu_{0.97}(BO_3)_2Cl:0.03Eu$ and $Ba_2(Lu_{0.97-z}Tb_z)(BO_3)_2Cl:0.03Eu$ phosphors with different Tb content (z values), and the Rietveld analysis patterns for X-ray powder diffraction data of $Ba_2Lu(BO_3)_2Cl$ (b) and $Ba_2Tb(BO_3)_2Cl$ (c) compounds.

$Ba_{1.97}Lu(BO_3)_2Cl:0.03Eu$ and $Ba_2(Lu_{0.97-z}Tb_z)(BO_3)_2Cl:0.03Eu$ phosphors. All of the XRD patterns are identical indicating the formation of a single phase with no impurity phases. Furthermore, Fig. 1b and 1c plot the experimental, calculated and difference results from the GSAS refinement of the two end components $Ba_2Lu(BO_3)_2Cl$ and $Ba_2Tb(BO_3)_2Cl$. The Rietveld analysis results indicate that the weighted profile R-factor (R_{wp}) and the expected R factor (R_p) are 12.52% and 9.47% for $Ba_2Lu(BO_3)_2Cl$, and 9.43% (R_{wp}), 6.93% (R_p) for $Ba_2Tb(BO_3)_2Cl$, respectively.[14] The above results confirm the phase purity of the as-prepared samples. Fig. S1† also shows the XRD patterns of $Ba_2(Y_{0.97-z}Tb_z)(BO_3)_2Cl:0.03Eu$ and $Ba_2(Gd_{0.97-z}Tb_z)(BO_3)_2Cl:0.03Eu$ phosphors with different Tb content. The observed XRD patterns confirm that all the $Ba_2Ln_{0.97-z}Tb_z(BO_3)_2Cl:0.03Eu$ (Ln = Y, Gd and Lu, z = 0–0.97) phosphors are single phase. These compounds crystallize as a monoclinic structure with space group $P2_1/m$ and $a \neq b \neq c$, $\alpha = \gamma = 90° \neq \beta$.[17] The lattice constants and cell volumes change depending on the relative ion radius of Ln/Tb (Ln = Y, Gd, Lu) according to Vegard's rule. The pure phase structure further guarantees that the ET of $Eu^{2+} \rightarrow (Tb^{3+})_n \rightarrow Eu^{3+}$ occurs in a single host lattice.

3.2 Tb content dependence of photoluminescence

Photoluminescence (PL) spectra of $Ba_{1.97}Lu(BO_3)_2Cl:0.03Eu$ and $Ba_2(Lu_{0.97-z}Tb_z)(BO_3)_2Cl:0.03Eu$ phosphors are shown in Fig. 2. It is found that $Ba_2Lu_{0.97}(BO_3)_2Cl:0.03Eu$ phosphors show green band emission with a maximum at about 512 nm. The observed broad-band emission is attributed to the $4f^65d–4f^7$ transitions of the Eu^{2+} ions. With the introduction of a small amount of Tb (z = 0.05), substitution for Lu in the host, the PL spectrum under excitation at 377 nm consists of green-emitting Tb^{3+} peaks located at about 488 and 543 nm (due to $^5D_4$ to $^7F_6$ and $^7F_5$ transitions) on top of the Eu^{2+} band emission.[18] The Eu^{2+} emission is dominant and both phosphors exhibit green emission upon 365 nm band excitation with a

Fig. 2 Emission spectra for 377 nm excitation of $Ba_{1.97}Lu(BO_3)_2Cl:0.03Eu$ and $Ba_2(Lu_{0.97-z}Tb_z)(BO_3)_2Cl:0.03Eu$ phosphors with different Tb content (z values).

UV lamp, as shown in the digital photographs (samples a and b in Fig. 3). When the Tb content is increased in the $Ba_2(Lu,Tb)(BO_3)_2Cl:0.03Eu$ phosphor, the relative intensities of the green Tb^{3+} emission lines increase gradually, while the broad-band emission decreases accordingly. Furthermore, when the Tb content reaches z = 0.3, emission peaks located at about 594, 612 and 624 nm (assigned to $^5D_0$ to $^7F_1$ and $^7F_2$ transitions of Eu^{3+}) appear to be accompanied by a decrease of the green Tb^{3+} emission at 543 nm, indicating the efficient ET between Tb^{3+} and Eu^{3+}.[19] We can explain the changes in the emission spectrum in Fig. 2 by ET of $Eu^{2+} \rightarrow (Tb^{3+})_n \rightarrow Eu^{3+}$, where $(Tb^{3+})_n$ signifies $Tb^{3+}–Tb^{3+}$ energy migration. It is found that Tb^{3+} emission is not completely quenched at z = 0.97 for the $Ba_2Tb_{0.97}(BO_3)_2Cl:0.03Eu$ phosphor (Fig. 2), indicating that both $Tb^{3+}–Tb^{3+}$ and $Tb^{3+}–Eu^{3+}$ ET are short-range in nature.[9] As is shown in Fig. S2,† similar changes in the emission spectra due to $Eu^{2+} \rightarrow (Tb^{3+})_n \rightarrow Eu^{3+}$ ET processes are also
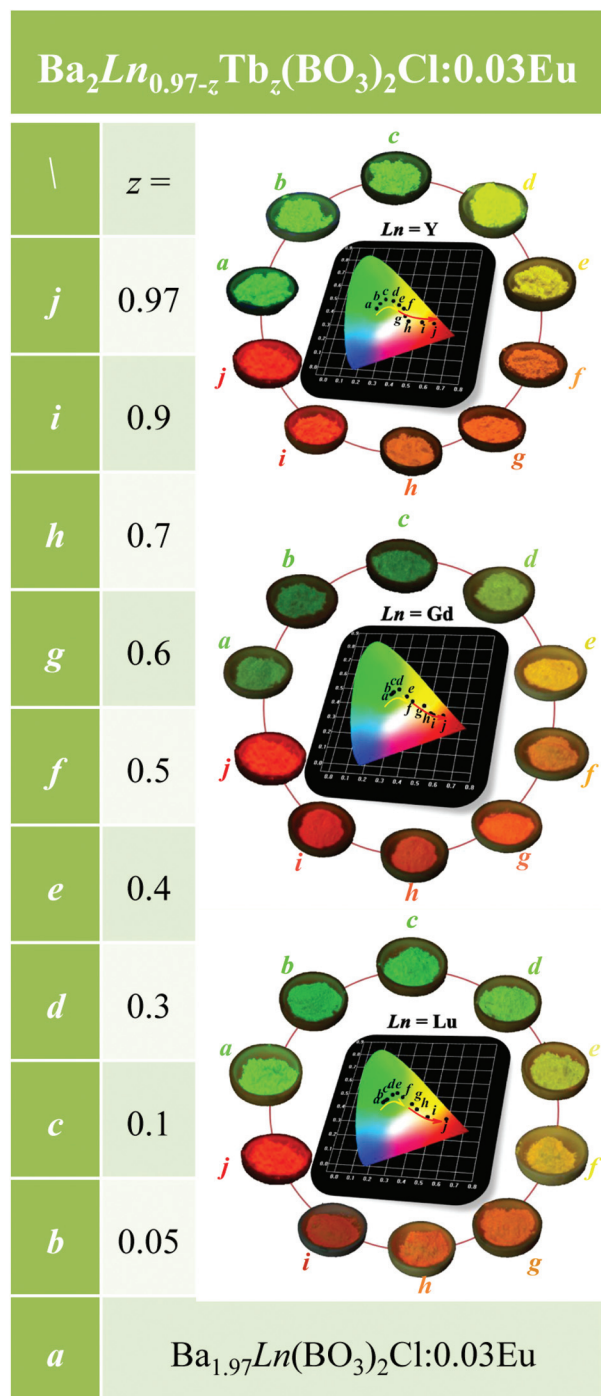
Fig. 3 Photographs upon a 365 nm UV lamp and the CIE chromaticity coordinates of $Ba_{1.97}Ln(BO_3)_2Cl:0.03Eu$ and $Ba_2(Ln_{0.97-z}Tb_z)(BO_3)_2Cl:Eu$ phosphors with different Tb content (z values).

found in the $Ba_2(Y_{0.97-z}Tb_z)(BO_3)_2Cl:0.03Eu$ and $Ba_2(Gd_{0.97-z}Tb_z)(BO_3)_2Cl:0.03Eu$ phosphors. The emission colors can be adjusted from the greenish yellow light of broad-band emissions of Eu^{2+} in $Ba_2Y_{0.97}(BO_3)_2Cl:0.03Eu$ and $Ba_2Gd_{0.97}(BO_3)_2Cl:0.03Eu$ to the red emission from Eu^{3+} via $Eu^{2+} \rightarrow (Tb^{3+})_n \rightarrow Eu^{3+}$ ET processes. The photographs in Fig. 3 illustrate the color-tunability upon a 365 nm excitation with a UV lamp for

$Ba_{1.97}Ln(BO_3)_2Cl:0.03Eu$ and $Ba_2(Ln_{0.97-z}Tb_z)(BO_3)_2Cl:Eu$ phosphors with different Tb content. The variation in color can be clearly observed by the naked eye. The CIE chromaticity coordinates of the three series of $Ba_2(Ln_{0.97-z}Tb_z)(BO_3)_2Cl:Eu$ phosphors are marked in the CIE diagram, and it clearly shows the variation of the emission colors depending on the Tb content in the host compositions. The color coordinates are listed in Table 1 for the selected samples. It is interesting to realize that the color tunable emissions via the host substitution of Tb/Ln (Ln = Y, Gd, Lu) occur for a fixed Eu-concentration of 3 mol%. Furthermore, the corresponding fractions of the total emission intensities in every composition assigned to Eu^{2+}, Tb^{3+} and Eu^{3+} are also given in Table 1.

3.3 Energy transfer processes

The energy transfer of Tb^{3+} to Eu^{3+} has been studied intensively, and the color output of Eu^{3+} and Tb^{3+} can be easily tuned by the excitation wavelength, as demonstrated in some recent references.[20] In the present case, in order to better understand the mechanism behind the adjustable emission colors from Eu^{2+}, Tb^{3+} and Eu^{3+} in the single-phase $Ba_2(Ln_{0.97-z}Tb_z)(BO_3)_2Cl:Eu$ phosphors, a typical composition, viz. $Ba_2Lu_{0.57}Tb_{0.4}(BO_3)_2Cl:0.03Eu$, was selected, and excitation and emission spectra were recorded. Fig. 4 shows excitation spectra monitoring 512, 543 and 594 nm emission and an emission spectrum under 377 nm excitation. The PL spectrum shows band-emission of Eu^{2+} and line-emissions of Tb^{3+} and Eu^{3+}. The 512 nm band emission is due to the $4f^65d–4f^7(^8S_{7/2})$ transition of Eu^{2+}, while the 488 and 543 nm peaked line-emissions are due to $^5D_4–^7F_{6,5}$ transitions of Tb^{3+}, and the 594, 612 and 618 nm peaked line-emissions to $^5D_0–^7F_{1,2}$ transitions of Eu^{3+}. The photoluminescence excitation (PLE) spectra while monitoring Eu^{3+} emission at 594 and Tb^{3+} emission at 543 nm give similar spectral profiles and show excitation lines due to f–f transitions on the Tb^{3+} ion between 300 and 380 nm, which is direct evidence of $Tb^{3+}–Eu^{3+}$ ET.[19b] More importantly, it is found that there are strong and broad absorption bands in the n-UV and violet region (300–450 nm) for the excitation spectra monitoring both the Tb^{3+} and Eu^{3+} emissions, which are similar to the excitation bands observed while monitoring Eu^{2+} emission at 512 nm. The broad bands in the 300–450 nm range are assigned to $4f^7–4f^65d$ transitions on Eu^{2+} and the observation of these bands in the excitation spectra for Tb^{3+} and Eu^{3+} emission provides evidence for energy transfer from Eu^{2+} to Tb^{3+} in $Ba_2Lu_{0.57}Tb_{0.4}(BO_3)_2Cl:0.03Eu$. This series of excitation spectra demonstrates that $Tb^{3+}–Eu^{3+}$ ET occurs and also shows that the allowed Eu^{2+} 4f–5d absorption transition sensitizes Tb^{3+} and Eu^{3+} line emissions, which confirms the ET process of $Eu^{2+} \rightarrow (Tb^{3+})_n \rightarrow Eu^{3+}$. As shown in Fig. S3,† we also find the broad-band absorption in the 300–450 nm range in the excitation spectra for 594 nm emission in other $Ba_2(Lu_{0.97-z}Tb_z)(BO_3)_2Cl:0.03Eu$ phosphors, providing evidence for the same ET mechanism in this system. As a comparison, Fig. S4† shows the UV-vis diffuse reflectance spectra of $Ba_{1.97}Lu(BO_3)_2Cl:0.03Eu$ and $Ba_2(Lu_{0.97-z}Tb_z)(BO_3)_2Cl:0.03Eu$ phosphors with different Tb content. It is found that the

Table 1 CIE chromaticity coordinates, luminescence lifetimes of Eu^{2+} (5d–4f), Eu^{3+} ($^5D_0$–$^7F_2$) and Tb^{3+} ($^5D_4$–$^7F_5$) emissions, and quantum efficiency (QE) for $Ba_{1.97}Ln(BO_3)_2Cl:0.03Eu$ and $Ba_2(Ln_{0.97−z}Tb_z)(BO_3)_2Cl:0.03Eu$ phosphors with different Tb content z

$Ba_2Ln_{0.97−z}Tb_z(BO_3)_2Cl:0.03Eu$ sample compositions		CIE (x, y)	Emission fraction			Lifetimes			QE
			Eu^{2+}	Tb^{3+}	Eu^{3+}	Eu^{2+} (μs)	Tb^{3+} (ms)	Eu^{3+} (ms)	
Ln = Y	$z = 0^a$	(0.217, 0.439)	1.00	0	0	1.71	—	—	40%
	$z = 0.1$	(0.262, 0.506)	0.63	0.35	0.02	1.56	2.4	—	24%
	$z = 0.3$	(0.309, 0.499)	0.34	0.58	0.08	1.51	2.2	3.3	25%
	$z = 0.5$	(0.384, 0.445)	0.01	0.65	0.34	1.43	1.6	3.6	26%
	$z = 0.7$	(0.432, 0.350)	0	0.26	0.74	1.32	0.15	3.0	18%
	$z = 0.9$	(0.523, 0.347)	0	0.12	0.88	1.25	0.07	2.8	15%
Ln = Gd	$z = 0^a$	(0.261, 0.482)	1.00	0	0	1.92	—	—	18%
	$z = 0.1$	(0.262, 0.482)	0.31	0.67	0.02	1.87	2.4	—	16%
	$z = 0.3$	(0.294, 0.503)	0.14	0.71	0.15	1.68	2.0	3.5	36%
	$z = 0.5$	(0.387, 0.427)	0.07	0.46	0.47	1.60	0.5	3.2	30%
	$z = 0.7$	(0.512, 0.352)	0.02	0.28	0.70	1.53	0.1	2.8	45%
	$z = 0.9$	(0.533, 0.344)	0	0.05	0.95	1.10	0.07	2.7	63%
Ln = Lu	$z = 0^a$	(0.182, 0.447)	1.00	0	0	1.60	—	—	14%
	$z = 0.1$	(0.232, 0.483)	0.68	0.31	0.01	1.42	2.0	—	31%
	$z = 0.3$	(0.251, 0.504)	0.32	0.58	0.10	1.35	1.7	4.0	44%
	$z = 0.5$	(0.295, 0.484)	0.35	0.45	0.30	1.29	0.6	4.2	51%
	$z = 0.7$	(0.399, 0.402)	0.03	0.34	0.63	1.11	0.3	3.0	71%
	$z = 0.9$	(0.471, 0.353)	0	0.04	0.96	1.01	0.15	2.9	73%
$Ba_2Tb_{0.97}(BO_3)_2Cl:0.03Eu$		(0.588, 0.345)	0	0.03	0.97	0.11	0.05	2.7	74%

^{a} When $z = 0$, the compounds are $Ba_{1.97}Ln(BO_3)_2Cl:0.03Eu$ (Ln = Y, Gd and Lu), respectively.
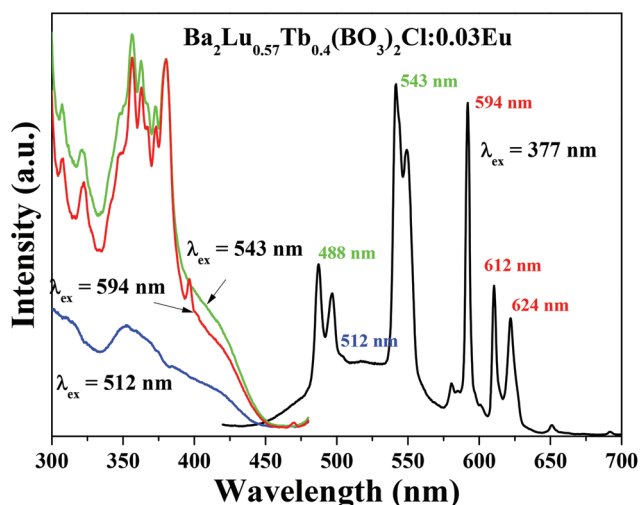
Fig. 4 Excitation spectra for emission at 512, 543 and 594 nm and emission spectrum under 377 nm excitation of $Ba_2Lu_{0.57}Tb_{0.4}(BO_3)_2Cl:0.03Eu$.

existence of Eu^{2+} in this series of $Ba_2(Lu_{0.97−z}Tb_z)(BO_3)_2Cl:0.03Eu$ phosphors can help to enhance the n-UV light absorption.

In general, the existence of Eu^{2+}, Tb^{3+} and Eu^{3+} in $Ba_2(Ln_{0.97−z}Tb_z)(BO_3)_2Cl:Eu$ phosphors can be verified from their characteristic PL and PLE spectra. However, the ratio Eu^{2+}/Eu^{3+} may vary between phosphors and it is important that the valence state of Eu can be controlled in a reproducible way since variations will lead to color changes. The relative amounts of Eu^{2+} and Eu^{3+} cannot be easily determined. The ionic radii of Eu^{2+} (0.117 nm), Eu^{3+} (0.095 nm), Tb^{3+} (0.092 nm), Y^{3+} (0.089 nm), Gd^{3+} (0.094 nm), and Lu^{3+} (0.085 nm) are very close to each other, the effect of the size

difference of the host cations on the stability of Eu ions is expected to be small. In order to further check the existence of different valence states of Eu and the variation of the ratio in $Ba_2(Ln_{0.97−z}Tb_z)(BO_3)_2Cl:Eu$ phosphors depending on the Tb/Ln substitution, ESR spectroscopy can provide information about the concentration and surroundings of the Eu^{2+} ions. The difference between the electronic configuration of Eu^{2+} and Eu^{3+} makes the Eu^{2+} ion paramagnetic in the $^8S_{7/2}$ ground state ($4f^7$, $S = 7/2$, $L = 0$, $J = 7/2$), while the Eu^{3+} ion is diamagnetic in the $^7F_0$ ground state ($4f^6$, $S = 3$, $L = 3$, $J = 0$).[21] Fig. S5† depicts the ESR spectra of $Ba_2Lu_{0.97}(BO_3)_2Cl:0.03Eu$ and $Ba_2(Lu_{0.97−z}Tb_z)(BO_3)_2Cl:Eu$ phosphors with different Tb content (z values). The difference in the ESR signals can be attributed to either the changes in the local surroundings or the Eu^{2+} concentration in the host lattice with Tb/Ln substitution, but it is hard to derive quantitative information on the 2+/3+ ratio from these spectra.

From the PLE and PL spectra in the selected $Ba_2Lu_{0.57}Tb_{0.4}(BO_3)_2Cl:0.03Eu$ phosphor (Fig. 4), it is clear that Eu^{2+}, Tb^{3+} and Eu^{3+} coexist in the single-phase $Ba_2(Ln_{0.97−z}Tb_z)(BO_3)_2Cl:Eu$ phosphors and that Eu^{3+} emission can be sensitized by Eu^{2+} *via* energy transfer involving Tb^{3+} ions. To learn more about the dynamics of ET processes, luminescence decay curves were recorded. Panels a–c in Fig. 5 give the luminescence decay curves of emission from Eu^{2+} (5d–4f), Tb^{3+} ($^5D_4$–$^7F_5$) and Eu^{3+} ($^5D_0$–$^7F_2$) in $Ba_2(Lu_{0.97−z}Tb_z)(BO_3)_2Cl:0.03Eu$ phosphors with different Tb content (z values). For the Eu^{2+} emission at 512 nm in the $Ba_2Lu_{0.97}(BO_3)_2Cl:0.03Eu$ phosphor a close to single exponential decay is observed with a lifetime of 1.6 μs, which is similar to the reported data in our previous work.[13] A value of 1.6 μs is within the range expected for Eu^{2+} in the green spectral region. Radiative lifetimes between 1 and 1.7 have been reported for Eu^{2+} emission around
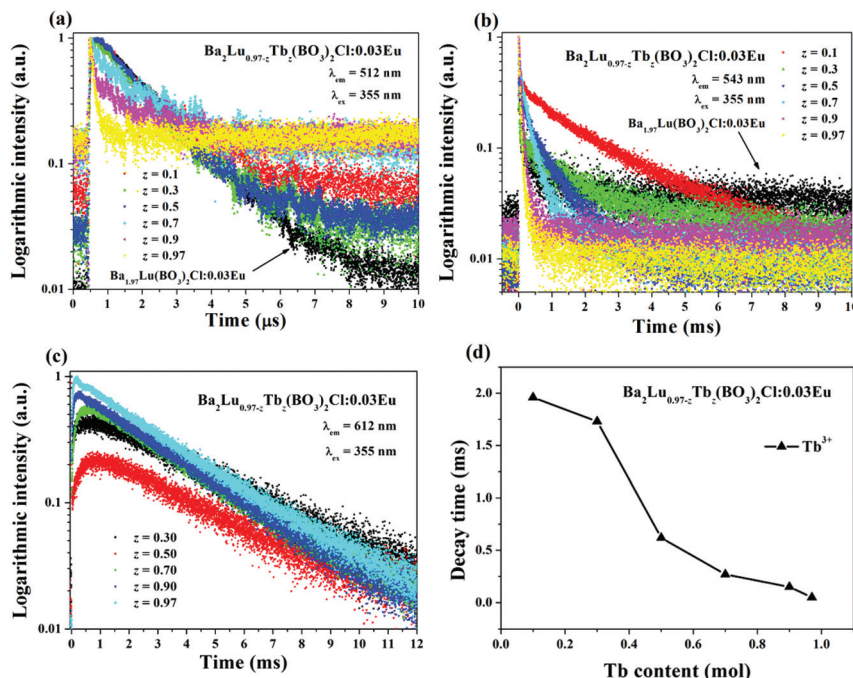
Fig. 5 Luminescence decay curves of Eu^{2+} (5d–4f) (a), Tb^{3+} ($^5D_4$–$^7F_5$) (b) and Eu^{3+} ($^5D_0$–$^7F_2$) (c) emission for $Ba_2(Lu_{0.97-z}Tb_z)(BO_3)_2Cl:0.03Eu$ phosphors with different Tb content (z values). The excitation and emission wavelengths for which the decay curves have been recorded are indicated in the figures. The variation of the lifetimes of the Tb^{3+} emission as a function of Tb content is also given (d).

510–520 nm.[22] As shown in panel a in Fig. 5, substitution of Tb for Lu in the host results in faster and non-exponential decay, which is attributed to ET from Eu^{2+} ions to neighboring Tb^{3+} ions. The lifetime of Eu^{2+} decreases with increasing Tb^{3+} content due to more efficient ET between Eu^{2+} and Tb^{3+} especially for higher Tb-concentrations. It is clear from the decay curves that for $z = 0.3$ or 0.5, the transfer is not complete as non-exponential decay curves can be observed. The very fast decay and low signal intensity observed for $z = 0.7$, 0.9 and 0.97 indicate that the energy transfer is almost complete. These observations are consistent with the emission spectra shown in Fig. 2 where the Eu^{2+} can hardly be observed for Tb-concentrations above 60%. A detailed analysis of the decay curves is beyond the scope of this work.

For the Tb^{3+} emission at 543 nm in the $Ba_2(Lu_{0.97-z}Tb_z)$ $(BO_3)_2Cl:0.03Eu$ phosphor, the decay curves are nonexponential for all Tb-concentrations (panel b in Fig. 5). The decay times of these samples are characterized by average lifetime (τ), which can be calculated by using the following equation,[23]

$$\tau = \frac{\int_0^\infty I(t)t\,dt}{\int_0^\infty I(t)\,dt} \quad (1)$$

where $I(t)$ represents the luminescence intensity at a time t. On the basis of eqn (1), the average lifetime values of Tb^{3+} at 543 nm in the series of $Ba_2(Lu_{0.97-z}Tb_z)(BO_3)_2Cl:0.03Eu$ phosphors were calculated to be 2.0, 1.7, 0.6, 0.3, 0.15 and 0.05 ms for $Ba_2(Lu_{0.97-z}Tb_z)(BO_3)_2Cl:0.03Eu$ phosphors at $z = 0.1$, 0.3, 0.5, 0.7, 0.9 and 0.97, respectively (Table 1). The rapid decrease in lifetime of Tb^{3+} emission is due to enhanced energy

migration over the Tb^{3+} sublattice. For $z = 0.1$ the energy migration will be limited as most Tb^{3+} ions will not have two Tb^{3+} nearest neighbors. The lifetime of 2.0 ms will be close to the radiative lifetime of the Tb^{3+} emission. For $z = 0.3$ the energy migration will still be limited but at $z = 0.5$ the Tb-concentration is close to the percolation point and rapid energy migration followed by energy transfer to Eu^{3+} ions acting as traps for the excitation energy explains the rapid drop in decay at the higher Tb-concentrations. Panel c in Fig. 5 gives the decay curves for the Eu^{3+} emission at 612 nm in the $Ba_2(Lu_{0.97-z}Tb_z)(BO_3)_2Cl:0.03Eu$ phosphor. The decay curves show a clear rise immediately after the excitation pulse which indicates feeding of the Eu^{3+} excited states. This confirms the ET mechanism involving energy migration over the Tb^{3+} sublattice and trapping of the excitation energy by Eu^{3+}. The rise is slow for a Tb-concentration of 30% when energy migration is hampered and becomes faster upon raising the Tb-concentration, in good agreement with the shortening of the lifetimes measured for the Tb^{3+} emission upon raising the Tb concentration. For the highest Tb fractions (90 and 97%) the rise is almost instantaneous, giving evidence for efficient energy migration over the Tb-lattice and fast and efficient trapping by Eu^{3+}. The decay of the Eu^{3+} emission is close to single exponential, but in view of a small deviation from a single exponential, the decay curves were well fitted with a biexponential equation,[24]

$$I = A_1 \exp(-t/\tau_1) + A_2 \exp(-t/\tau_2) \quad (2)$$

where I is the luminescence intensity at time t, t is the time, A_1 and A_2 are constants, and τ_1 and τ_2 are the decay times for the

exponential components. An average lifetime (τ^*) was determined from

$$\tau^* = (A_1\tau_1{}^2 + A_2\tau_1{}^2)/(A_1\tau_1 + A_2\tau_1) \qquad (3)$$

The average lifetime values of Eu^{3+} at 612 nm in this series of $Ba_2(Lu_{0.97-z}Tb_z)(BO_3)_2Cl:0.03Eu$ phosphors were calculated to be 4.0, 4.2, 3.0, 2.9 and 2.7 ms for $Ba_2(Lu_{0.97-z}Tb_z)$-$(BO_3)_2Cl:0.03Eu$ phosphors at z = 0.3, 0.5, 0.7, 0.9 and 0.97, respectively (Table 1). The long lifetime of 4.0 ms is consistent with the relatively high intensity of the magnetic dipole (MD) $^5D_0 \rightarrow {}^7F_1$ transition at 594 nm. The low intensities of the forced electric dipole (ED) transitions $^5D_0 \rightarrow {}^7F_{2,4}$ (around 620 and 700 nm, respectively) show that the contribution of forced ED transition to the total decay is limited and explain the long lifetime. The lifetime decreases from 4.0 ms to 2.8 ms upon raising the Tb-concentration. This observation shows that the local surroundings change in a subtle manner upon replacement of Lu by Tb, leading to a slightly higher forced ED transition probability. It is well known that forced ED transitions are very sensitive to small changes in the local surroundings. The sensitivity to the local surroundings can also explain the slight variation from a single exponential decay of the Eu^{3+} emission, where a single exponential is expected based on the presence of a single crystallographic site for Eu^{3+}. The local distribution of Tb and Lu around Eu^{3+} will vary due to a random Tb/Lu substitution. Different surroundings give rise to slightly different lifetimes. Table 1 lists all the selected lifetimes of Eu^{2+} (5d–4f), Eu^{3+} ($^5D_0-{}^7F_2$) and Tb^{3+} ($^5D_4-{}^7F_5$) emissions in the $Ba_2(Lu_{0.97-z}Tb_z)(BO_3)_2Cl:0.03Eu$ phosphors with different Tb content. The luminescence decay dynamics confirm the ET mechanism $Eu^{2+} \rightarrow (Tb^{3+})_n \rightarrow Eu^{3+}$. Parameters determined from similar luminescence decay curves measured for $Ba_2(Y_{0.97-z}Tb_z)(BO_3)_2Cl:0.03Eu$ and $Ba_2(Gd_{0.97-z}Tb_z)$-$(BO_3)_2Cl:0.03Eu$ are also included, based on the analysis of their corresponding decay curves, given in Fig. S6 and S7.†

It is interesting to investigate the first energy transfer step $Eu^{2+} \rightarrow Tb^{3+}$ in more detail. As proposed by Blasse, the critical distance for ET (R_c) between donor and acceptor can be estimated from the acceptor concentration at which the donor emission intensity has dropped to half the initial intensity. For this acceptor concentration the probability for energy transfer is equal to the radiative decay rate for the donor emission. The critical distance for energy transfer $R_{Eu^{3+}-Tb^{3+}}$ between Eu^{3+} and Tb^{3+} can be estimated by the following formula,[25]

$$R_c \approx 2\left(\frac{3V}{4\pi\,x_cN}\right)^{1/3} \qquad (4)$$

where V is the volume of the unit cell and N is the number of host cations in the unit cell. The $Ba_2Lu(BO_3)_2Cl$ compound has monoclinic structure with the cell volume V = 386.810 Å^3 and N = 2. x_c is the acceptor concentration (here the Tb^{3+} concentration) for which the donor (Eu^{2+}) emission has dropped to half the initial intensity. From the emission spectra in Fig. 2, x_c has been determined to be between 0.3 and 0.4. The critical transfer distance R_c for Eu^{2+}–Tb^{3+} ET in $Ba_2(Lu_{0.97-z}$-

$Tb_z)(BO_3)_2Cl:Eu$ is calculated to be about 10 Å, which is large for energy transfer from an allowed donor to a forbidden acceptor transition.

The QE values of phosphors are very important for application.[26] For application as phosphors in light emitting devices like w-LEDs, QEs close to unity are required. We measured the QEs for the various phosphors and Table 1 summarizes the internal QE values. The QE values of the $Ba_{1.97}Ln$-$(BO_3)_2Cl:0.03Eu$ (Ln = Y, Gd, and Lu) phosphors measured under 352 nm excitation for emission in the range of 362–694 nm are 40%, 18% and 14%, respectively. The measurement conditions for the $Ba_2Ln_{0.97-z}Tb_z(BO_3)_2Cl:0.03Eu$ phosphors were done for excitation at 377 nm and emission in the range of 367–744 nm. It is found that the QE values of $Ba_2Y_{0.97-z}Tb_z(BO_3)_2Cl:0.03Eu$ phosphors initially decrease with the introduction of Tb, and then stay at a relatively low value of 15%–25%. However, the QE values of $Ba_2Ln_{0.97-z}Tb_z(BO_3)_2$-$Cl:0.03Eu$ (Ln = Gd and Lu) increase with increasing Tb content in the host. The QE value of the red-emitting $Ba_2Tb_{0.97}(BO_3)_2Cl:0.03Eu$ phosphor is 74%, which is a little higher than previously reported owing to the different emission range collected by the photomultiplier tube.[14] The measured QEs of the $Ba_2Ln_{0.97-z}Tb_z(BO_3)_2Cl:0.03Eu$ phosphors are relatively high, and can be further enhanced by optimization of the synthesis conditions and the compositions.[26]

3.4 Temperature dependent luminescence properties

Thermal quenching is an important consideration for the application of phosphors in w-LEDs.[27] Fig. 6 gives the temperature dependence of PL spectra for the selected three samples of $Ba_2(Ln_{0.47}Tb_{0.5})(BO_3)_2Cl:0.03Eu$ (Ln = Y, Gd, and Lu) and $Ba_2Tb_{0.97}(BO_3)_2Cl:0.03Eu$ phosphors. Both the Tb^{3+} emission lines (at 543 nm) and the Eu^{3+} emission lines (at 594, 612 and 624 nm) can be found from the PL spectra. The PL intensities from Eu^{3+} emission for all the samples decrease with increasing temperature. For the PL intensities from the Tb^{3+} emission, it is found that the PL intensities of $Ba_2(Y_{0.47}Tb_{0.5})$-$(BO_3)_2Cl:0.03Eu$ (abbreviated as BYTE), $Ba_2(Gd_{0.47}Tb_{0.5})$-$(BO_3)_2Cl:0.03Eu$ (BGTE) and $Ba_2Tb_{0.97}(BO_3)_2Cl:0.03Eu$ phosphors increase with increasing temperature from room temperature, which is an unusual but interesting phenomenon. Fig. 7 gives the temperature dependence of the PL intensities of Eu^{3+} ($^5D_0-{}^7F_2$) transitions at 594 nm and Tb^{3+} ($^5D_4-{}^7F_5$) transitions at 543 nm for BYTE, BGTE, $Ba_2(Lu_{0.47}Tb_{0.5})$-$(BO_3)_2Cl:0.03Eu$ (BLTE), and $Ba_2Tb_{0.97}(BO_3)_2Cl:0.03Eu$ phosphors, respectively. At 150 °C, the red emission intensity at 594 nm is found to be 84.7%, 90.0%, 63.4% and 79.2% of the initial value for BYTE, BGTE, BLTE and $Ba_2Tb_{0.97}(BO_3)_2$-$Cl:0.03Eu$, respectively. This shows that this series of phosphors demonstrated favorable thermal quenching behavior, which is consistent with our previous report on the Ba_2Ln-$(BO_3)_2Cl:Eu^{2+}$ (Ln = Y, Gd and Lu) phosphors.[13]
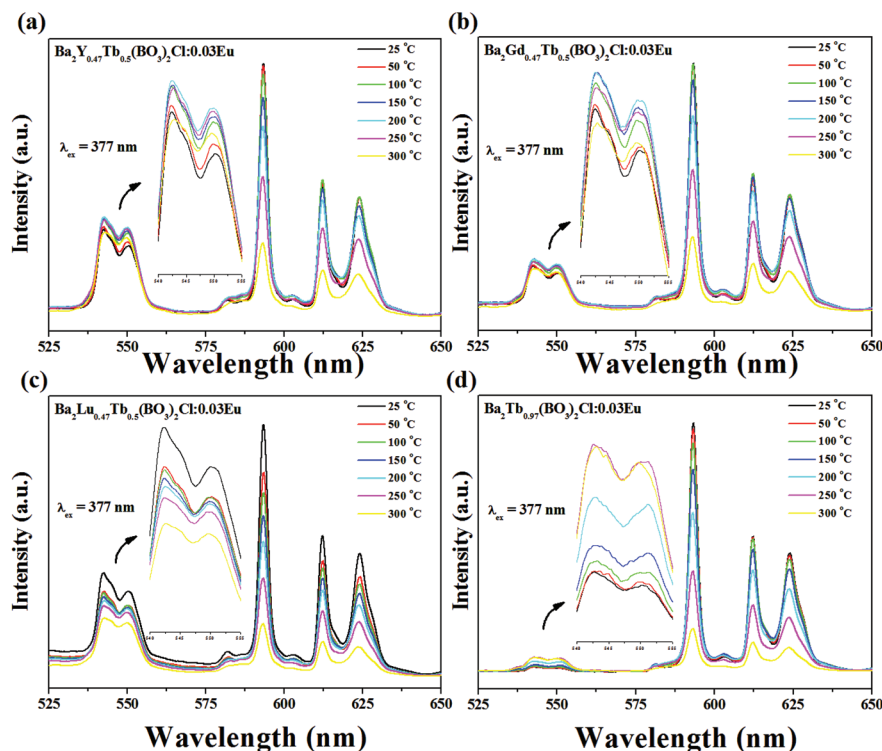
Fig. 6 Temperature dependence of PL spectra for the selected $Ba_2(Ln_{0.47}Tb_{0.5})(BO_3)_2Cl:0.03Eu$ and $Ba_2Tb_{0.97}(BO_3)_2Cl:0.03Eu$ phosphors.
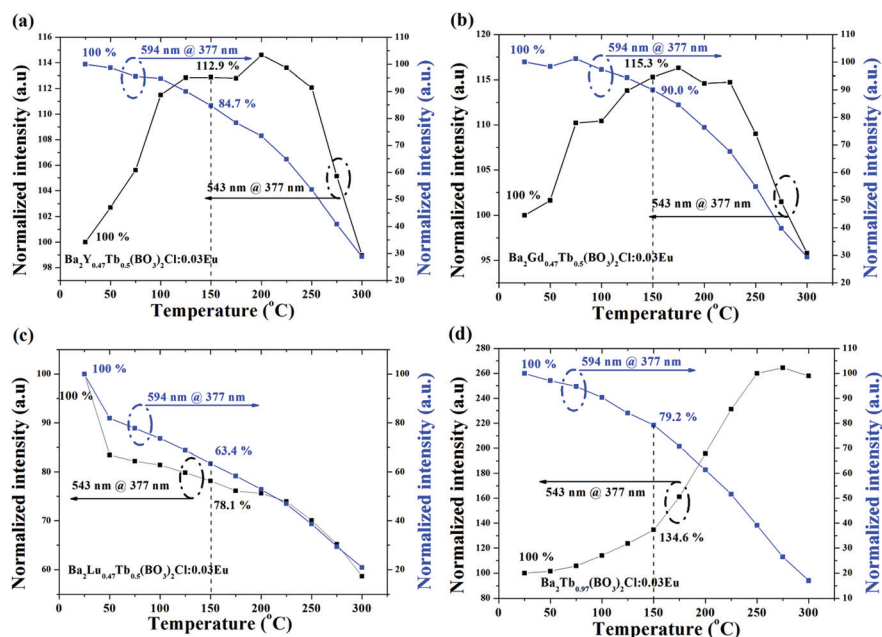
Fig. 7 Variation of Eu^{3+} ($^5D_0-^7F_2$) transitions at 594 nm and Tb^{3+} ($^5D_4-^7F_5$) transitions at 543 nm for $Ba_2(Y_{0.47}Tb_{0.5})(BO_3)_2Cl:0.03Eu$ (a), $Ba_2(Gd_{0.47}Tb_{0.5})$-$(BO_3)_2Cl:0.03Eu$ (b), $Ba_2(Lu_{0.47}Tb_{0.5})(BO_3)_2Cl:0.03Eu$ (c) and $Ba_2Tb_{0.97}(BO_3)_2Cl:0.03Eu$ (d) phosphors.

4. Conclusions

Efficient and color-tunable emission has been realized in a single-phase phosphor $Ba_2Ln_{0.97-z}Tb_z(BO_3)_2Cl:0.03Eu$ (Ln = Y, Gd and Lu, z = 0–0.97) where the emission color can be varied between green and red depending on the relative content of Tb in the host. The single-phase composition design strategy relies on the presence of both Eu^{2+} and Eu^{3+} and uses the allowed Eu^{2+} absorption to sensitize Eu^{3+} line emission *via* the ET mechanism $Eu^{2+} \rightarrow (Tb^{3+})_n \rightarrow Eu^{3+}$. The

photoluminescence properties have been determined by analysis of the luminescence spectra, decay kinetics, quantum efficiency, thermal quenching and CIE chromaticity index. This study indicates that the host lattices with a divalent alkaline earth and a trivalent lanthanide site can be used to sensitize Eu^{3+} emission using allowed Eu^{2+} absorption transitions in the *n*-UV and violet region, and yield color tunable phosphors for application in solid-state *w*-LEDs.

Notes and references

1 (*a*) S. Nakamura and G. Fasol, *The Blue Laser Diode*, Springer, Berlin, Germany, 1996; (*b*) C. C. Lin and R. S. Liu, *J. Phys. Chem. Lett.*, 2011, **11**, 1268; (*c*) V. Bachmann, C. Ronda and A. Meijerink, *Chem. Mater.*, 2009, **21**, 2077.

2 (*a*) S. Ye, F. Xiao, Y. X. Pan, Y. Y. Ma and Q. Y. Zhang, *Mater. Sci. Eng., R*, 2010, **71**, 1; (*b*) H. A. Höppe, *Angew. Chem., Int. Ed.*, 2009, **48**, 3572; (*c*) Z. G. Xia, H. Y. Du, J. Y. Sun, D. M. Chen and X. F. Wang, *Mater. Chem. Phys.*, 2010, **119**, 7.

3 (*a*) G. Blasse and B. C. Grabmaier, *Luminescent Materials*, Springer-Verlag, Berlin, 1994; (*b*) P. Dorenbos, *J. Lumin.*, 2000, **91**, 155; (*c*) Y. Q. Li, A. C. A. Deising, G. de With and H. T. Hintzen, *Chem. Mater.*, 2005, **17**, 3242; (*d*) J. Liu, H. Z. Lian and C. S. Shi, *Opt. Mater.*, 2007, **29**, 1591.

4 (*a*) W. T. Chen, H. S. Sheu, R. S. Liu and J. P. Attfield, *J. Am. Chem. Soc.*, 2012, **134**, 8022; (*b*) Z. G. Xia, J. Y. Sun, H. Y. Du and W. Zhou, *Opt. Mater.*, 2006, **28**, 524; (*c*) Z. G. Xia, Q. Li and J. Y. Sun, *Mater. Lett.*, 2007, **61**, 1885; (*d*) M. Zeuner, F. Hintze and W. Schnick, *Chem. Mater.*, 2009, **21**, 336.

5 (*a*) H. A. Höoppe, F. Stadler, O. Oeckler and W. Schnick, *Angew. Chem., Int. Ed.*, 2004, **43**, 5540; (*b*) R. J. Xie and N. Hirosaki, *Sci. Technol. Adv. Mater.*, 2007, **8**, 588; (*c*) H. Nersisyan, H. I. Won and C. W. Won, *Chem. Commun.*, 2011, **47**, 11897.

6 (*a*) F. P. Du, R. Zhu, Y. L. Huang, Y. Tao and H. J. Seo, *Dalton Trans.*, 2011, **40**, 11433; (*b*) D. Kang, H. S. Yoo, S. H. Jung, H. Kim and D. Y. Jeon, *J. Phys. Chem. C*, 2011, **115**, 24334.

7 (*a*) J. G. Wang, X. P. Jing, C. H. Yan, J. H. Lin and F. H. Liao, *J. Lumin.*, 2006, **121**, 57; (*b*) B. Yan and J. H. Wu,

Mater. Chem. Phys., 2009, **116**, 67; (*c*) Z. G. Xia, J. F. Sun, H. Y. Du, D. M. Chen and J. Y. Sun, *J. Mater. Sci.*, 2010, **45**, 1553.

8 (*a*) X. Wu, Y. Huang, L. Shi and H. J. Seo, *Mater. Chem. Phys.*, 2009, **116**, 449; (*b*) A. R. Dhobale, M. Mohapatra, V. Natarajan and S. V. Godbole, *J. Lumin.*, 2012, **132**, 293.

9 A. A. Setlur, *Electrochem. Solid-State Lett.*, 2012, **15**, J25.

10 (*a*) P. Dorenbos, *Chem. Mater.*, 2005, **17**, 6452; (*b*) Z. Song, J. Liao, X. L. Ding, T. L. Zhou and Q. L. Liu, *J. Lumin.*, 2012, **132**, 1768; (*c*) M. P. Saradhi, V. Pralong, U. V. Varadaraju and B. Raveau, *Chem. Mater.*, 2009, **21**, 1793; (*d*) K. W. Huang, W. T. Chen, C. I. Chu, S. F. Hu, H. S. Sheu, B. M. Cheng, J. M. Chen and R. S. Liu, *Chem. Mater.*, 2012, **24**, 2220.

11 (*a*) Q. Su, H. B. Liang, T. D. Hu, Y. Tao and T. Liu, *J. Alloys Compd.*, 2002, **344**, 132; (*b*) Z. Y. Mao, D. J. Wang, Q. F. Lu, W. H. Yu and Z. H. Yuan, *Chem. Commun.*, 2009, 346; (*c*) M. P. Saradhi, S. Boudin, U. V. Varadaraju and B. Raveau, *J. Solid State Chem.*, 2010, **183**, 2496.

12 G. Blasse, *Phys. Status Solidi A*, 1983, **75**, K41.

13 Z. G. Xia, X. M. Wang, Y. X. Wang, L. B. Liao and X. P. Jing, *Inorg. Chem.*, 2011, **50**, 10134.

14 Z. G. Xia, J. Q. Zhuang and L. B. Liao, *Inorg. Chem.*, 2012, **51**, 7202.

15 Y. Gao and C. S. Shi, *J. Phys. Chem. Solids*, 1996, **157**, 1303.

16 (*a*) A. C. Larson and R. B. Von Dreele, *General Structure Analysis System (GSAS), Los Alamos National Laboratory Report LAUR 86-748*, Los Alamos National Laboratory, Los Alamos, NM, 1994; (*b*) B. H. Toby, *J. Appl. Crystallogr.*, 2001, **34**, 210.

17 (*a*) T. N. Khamaganova, N. N. Nevskii and V. K. Trunov, *Sov. Phys. Crystallogr.*, 1989, **34**, 853; (*b*) W. J. Schipper and G. Blasse, *J. Alloys Compd.*, 1994, **203**, 267; (*c*) Z. G. Xia, J. Q. Zhuang, L. B. Liao, H. K. Liu, Y. Luo and P. Du, *J. Electrochem. Soc.*, 2011, **158**, J359.

18 (*a*) W. Lu, Z. D. Hao, X. Zhang, Y. S. Luo, X. J. Wang and J. H. Zhang, *Inorg. Chem.*, 2011, **50**, 7846; (*b*) N. Guo, Y. H. Song, H. P. You, G. Jia, M. Yang, K. Liu, Y. H. Zheng, Y. J. Huang and H. J. Zhang, *Eur. J. Inorg. Chem.*, 2010, **29**, 4636.

19 (*a*) J. Yang, C. M. Zhang, C. X. Li and J. Lin, *Inorg. Chem.*, 2008, **47**, 7262; (*b*) M. Yu, H. Wang, C. K. Lin, G. Z. Li and J. Lin, *Nanotechnology*, 2006, **17**, 3245.

20 (*a*) T. S. Atabaev, H. K. Kim and Y. H. Hwang, *J. Lumin.*, 2012, **373**, 14; (*b*) D. Tu, Y. J. Liang, R. Liu and D. Y. Li, *J. Lumin.*, 2011, **131**, 2569.

21 (*a*) W. B. Im, Y. I. Kim and D. Y. Jeon, *Chem. Mater.*, 2006, **18**, 1190; (*b*) W. B. Im, J. H. Kang, D. C. Lee, S. Lee, D. Y. Jeon, Y. C. Kang and K. Y. Jung, *Solid State Commun.*, 2005, **133**, 197; (*c*) W. B. Im, Y. I. Kim, H. S. Yoo and D. Y. Jeon, *Inorg. Chem.*, 2009, **48**, 557.

22 S. H. M. Poort, A. Meijerink and G. Blasse, *J. Phys. Chem. Solids*, 1997, **58**, 1451.

23 (*a*) G. Blasse, *Philips Res. Rep.*, 1969, **24**, 131; (*b*) X. Liu, Y. Teng, Y. Zhuang, J. Xie, Y. Qiao, G. Dong, D. Chen and

J. Qiu, *Opt. Lett.*, 2009, **34**, 3565; (*c*) Y. C. Jia, H. Qiao, Y. H. Zheng, N. Guo and H. P. You, *Phys. Chem. Chem. Phys.*, 2012, **14**, 3537.

24 (*a*) C. H. Huang, T. M. Chen, W. R. Liu, Y. C. Chiu, Y. T. Yeh and S. M. Jang, *ACS Appl. Mater. Interfaces*, 2010, **2**, 259; (*b*) C. H. Huang and T. M. Chen, *J. Phys. Chem. C*, 2011, **115**, 2349.

25 (*a*) G. Blasse, *Philips Res. Rep.*, 1969, **24**, 131; (*b*) G. Blasse, *J. Solid State Chem.*, 1986, **62**, 207.

26 (*a*) A. Birkel, K. A. Denault, N. C. George, C. E. Doll, B. Hery, A. A. Mikhailovsky, C. S. Birkel, B. C. Hong and R. Seshadri, *Chem. Mater.*, 2012, **24**, 1198; (*b*) Z. G. Xia, R. S. Liu, K. W. Huang and V. Drozd, *J. Mater. Chem.*, 2012, **22**, 15183.

27 (*a*) D. Y. Wang, C. H. Huang, Y. C. Wu and T. M. Chen, *J. Mater. Chem.*, 2011, **21**, 10818; (*b*) J. Y. Han, W. B. Im, D. Kim, S. H. Cheong, G. Y. Lee and D. Y. Jeon, *J. Mater. Chem.*, 2012, **22**, 5374.